Optica Applicata, Vol. XXIII, No. 1, 1993

$InAs_{1-x}Sb_x$ room temperature magnetoconcentration photodetector for 10.6 μm radiation

W. GAWRON, J. PIOTROWSKI

Institute of Technical Physics, Military Academy of Technology, ul. S. Kaliskiego 2, 01-489 Warszawa Poland.

Performance of $InAs_{1-x}Sb_x$ room temperature magnetoconcentration photodetectors has been analysed. It has been shown that detectivity of $1\cdot 10^9$ cmHz$^{1/2}$/W can be achieved with lightly doped p-type material.

1. Introduction

The room temperature infrared detectors find increasing applications in industry, military and science. The removal of troublesome cooling widens their applicability to many new fields. A classic example is provided by photoconductors and photomagnetoelectrical detectors operated at room temperature, being now commercially available [1]. During recent years many works appeared devoted to the ways of increasing the working temperature of detectors and improving their parameters.

The performance of the ambient temperature infrared photodetectors is determined by a very high rate of thermal generation and recombination processes in narrow gap semiconductors. PIOTROWSKI and DJURIČ [2], [3] proposed to suppress the Auger generation and recombination by depleting the active region of the semiconductor using the magnetoconcentration effect [4]. This problem has been described in detail in recent papers [5], [6].

In this paper, it has been shown that a solid solution of $InAs_{1-x}Sb_x$ may be used to build a room temperature magnetoconcentration detector operating in the 8–14 μm atmosphere window. The energy gap of $InAs_{1-x}Sb_x$ changes with composition x [7]–[10], and it can be approximated by the formula [9]

$$E_g(x,T) = 0.411\frac{3.4\cdot 10^{-4}T^2}{210+T} - 0.876x + 0.70x^2 + 3.4\cdot 10^{-4}xT(1-x)$$

where E_g is the band gap (in eV), T is the temperature (in K).

According of the formula, the material with $x = 0.65$ has E_g equal to 0.1 at room temeprature and can be used for $\lambda = 10.6$ μm CO_2 laser radiation detectors.

The purpose of this work is to determine numerically the limiting parameters of room temperature magnetoconcentration photodetectors produced of $InAs_{0.35}Sb_{0.65}$ for the CO_2 laser radiation of the wavelength $\lambda = 10.6$ μm.

2. Theoretical model of a magnetoconcentration detector

Scheme of the magnetoconcentration detector is shown in Figure 1. Its construction is similar to that of conventional photoelectromagnetic detector. A thin semiconductor plate with two contacts is immersed in magnetic field. The upper (illuminated) surface of the semiconductor is passivated in order to obtain low surface re-

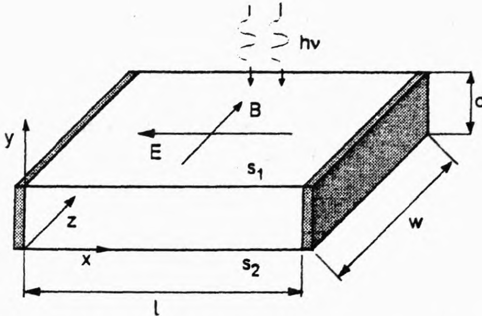

Fig. 1. Scheme of the magnetoconcentration photodetector (E – electric field, B – magnetic field, l, w, d – sizes of the sample, x, y, z – coordinates, hv – photon energy)

combination velocity s_1, while the lower (backside) surface has been suitably treated to obtain high surface recombination velocity s_2. The photoconductor is biased with an electric field perpendicular to the magnetic field and oriented in such a way that the Lorentz force, acting on the current carriers, sweeps them to the surface of high surface recombination velocity. As a results, the concentration of electrons and holes in the large part of the material is reduced and thus the region becomes depleted.

3. Numerical calculations

The calculations of magnetoconcentration detector parameters were performed by numerical solving of phenomenological transport equations and continuity equations for electrons and holes [5], [6]. All the calculations of the detector parameters were carried out under the assumption of the 300 K temperature, the $2T$ magnetic induction and the following sizes of the sample: $l = w = 100$ μm, $d = 5$ μm. The value of magnetic induction B was assumed to be $2T$ since this is a realistic value which may be achieved with a miniature permanent magnet. The parameters of the material necessary for calculations are presented in the Table. The depletion effect of the semiconductor due to the magnetoconcentration effect is shown in Fig. 2 as function of the applied electric field. As a result of Lorentz force, the concentration of both minority and majority carriers decreases with increasing electric field, except for the region in vicinity of the backside contact. At strong electrical fields ($>$ 200 V/cm), the concentration of majority carriers tends to saturate at extrinsic level, while the concentration of minority carriers still decreases. The depletion of

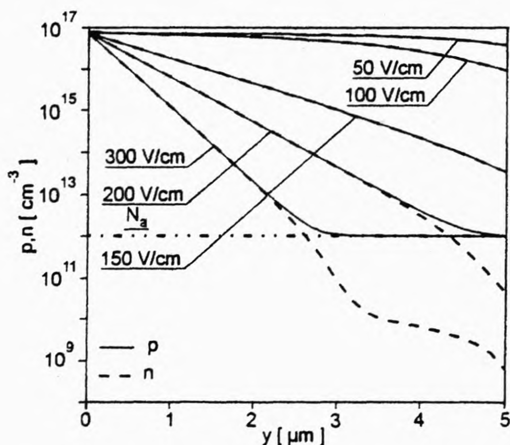

Fig. 2. Carrier concentration profile p, n across the semiconductor (coordinate y) for different values of the electric field E

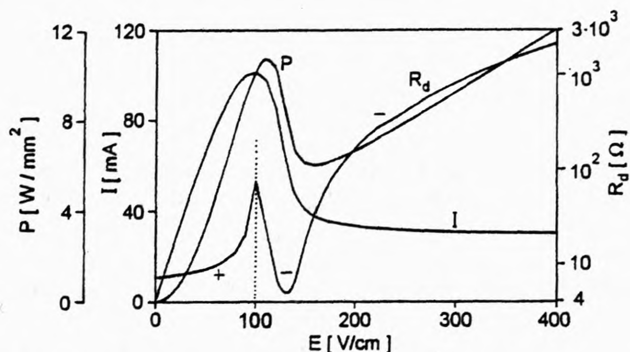

Fig. 3. Dependence of the dark current I, dynamic resistance R_d and the power P density on the electric field E

Table. Parameters of $InAs_{1-x}Sb_x$ [8]–[10]

Energy gap	E_g	0.112	eV
Electron mobility	μ_e	3.75	m^2/Vs
Hole mobility	μ_h	0.04	m^2/Vs
Auger 1 lifetime, intrinsic	τ_1^i	$3.5 \cdot 10^{-10}$	s
Auger 7 lifetime, intrinsic	τ_7^i	$6.5 \cdot 10^{-9}$	s
Intrinsic concentration	n_i	$7 \cdot 10^{22}$	m^{-3}
Dopant concentration	N_a	$1 \cdot 10^{18}$	m^{-3}
Coefficient of absorption velocity	α	80000	1/m
Surface recombination velocity on the back side	s_1	10000	m/s
Surface recombination velocity on the front side	s_2	0	m/s

semiconductor results in non-linear current voltage characteristics (Fig. 3). At low electric field the dark current increases with electric field achieving maximum value at about 100 V/cm. Further increase of the electric field causes a drop and

then saturation of the current resulting in a negative resistance region. This behaviour can be interpreted as a combined action of increasing electric field and decreasing carrier concentration on the dark current. The increase of the current at low fields is due to the increasing field with mostly unchanged concentration. The decrease and saturation of the current at high fields is a direct result of the depletion of semiconductor which cannot be fully compensated by increasing field. It should be noted that the dark current at high fields flows practically in a thin region close to the backside surface of the semiconductor.

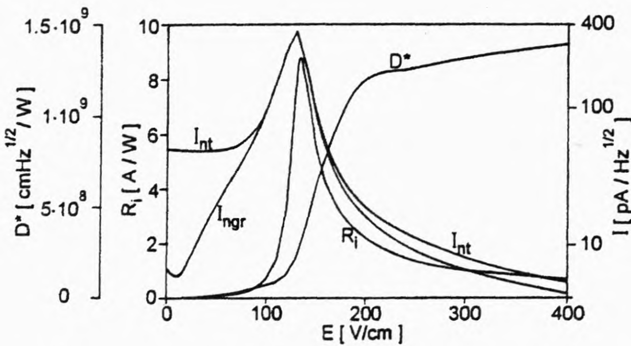

Fig. 4. Dependence of the current responsivity R_i, the generation-recombination noise current I_{ngr} and the total noise current, taking into account the Johnson noise ($I_{nt} = (I_{ngr}^2 + I_{nJ}^2)^{1/2}$) and the normalized detectivity D^*, on the electric field E

Figure 4 shows the dependence of the current responsivity R_i, the generation-recombination noise current I_{ngr} and the total noise, including the Johnson noise ($I_{nt} = (I_{ngr}^2 + I_{nJ}^2)^{1/2}$) and the normalized detectivity D^*, on the electric field E. With the increase of electric field the current responsivity increases, achieving maximum value for 130 V/cm. When the electric field increases further, a decrease of the photoelectrical gain occurs resulting in the lowering of the current responsivity. The generation-recombination noise behaves similarly, the relative decrease of the noise current at high field is much stronger compared to that of current responsivity. As a result, the normalized detectivity steadily increases with electric field. The dependence of the detector parameters on electric field can be explained considering in-depth distributions of the photoelectric gain g, the Auger generation rate G_A, the carrier concentrations n, p and the Auger noise current intensity I_n for low and high electric field (Figs. 5 and 6). The initial increase of current responsivity and noise current with electric field is due to increasing photoelectric gain, while the carriers concentrations and the Auger generation rate remain unchanged. The reduction of noise current at high fields is a direct result of dramatic suppression of the Auger generation rate in the major part of the detector due to depletion. Another important factor is the distribution of the photoelectric gain. The gain decreases towards backside surface. This dependence can be explained by the action of Lorentz force, which sweeps charge carriers in direction of high recombination velocity back

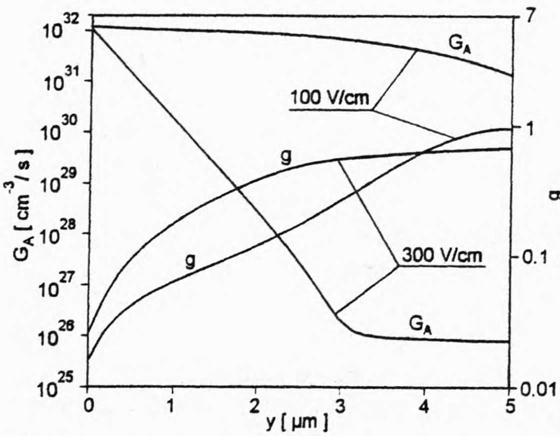

Fig. 5. Dependence of the Auger generation rate G_A and the photoelectric gain g on the position across semiconductor (coordinate y) for low and high electric fields

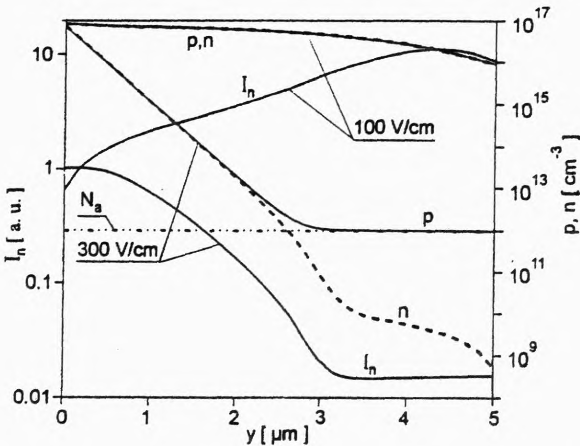

Fig. 6. Dependence of the carrier concentration n, p and the generation-recombination noise current density I_n on the position acrosss semiconductor (coordinate y) for low and high electric fields

surface. The effective lifetime is higher for carriers born far from that surface. Such a distribution of photoelectric gain is very beneficial for the performance of a device. The gain is high in the upper part of device, where optical carrier generation is strongest and noisy thermal generation is highly reduced.

At high electric fields, the total noise current is dominated by the less depleted region located close to the backside surface of the device, where thermal generation remains significant, despite of low photoelectric gain there. This region also dominates the dark current and bias power dissipation. When the electric field exceeds 200 V/cm, the increase of detectivity becomes modest. When a large part of the semiconductor is already depleted to the extrinsic level, the thermal generation

achieves its maximum value and the Johnson noise starts to dominate the total noise. In practice, the maximum electrical field applicable to the device is limited by Joule heating. As Figure 3 shows, the required depletion of semiconductor would require a very effective heat dissipation density of about 10 W/mm^2 with increase of temperature no more than a few K. Such a good heat dissipation can be achieved with sophisticated design of the device, for example, by cementing the semiconductor to substrate extreme thermal conductivity (*e.g.*, diamond) with a very thin layer of glue. The problem of heat dissipation becomes less stringent in the case of small area detectors, due to a three-dimensional heat dissipation.

Therefore, it has been proposed to apply the optical immersion of the photodetector to hemi- or hyperhemispherical lens of high refractive index n [11], [12], Fig. 7. The application of optical immersion results in an increase of optical size of the detector, compared to the actual linear size, by a large factor n- or n^2 for the hemi- and hyperhemispherical immersion. This directly improves the device detectivity by the same factors. The immersion lens can be produced directly from the substrate of epitaxial layer by the use of monolithic immersion technology, which has been developed at VIGO and already applied to improve performance of many types of photodetectors [1]. This technique makes it possible to achieve a very good heat

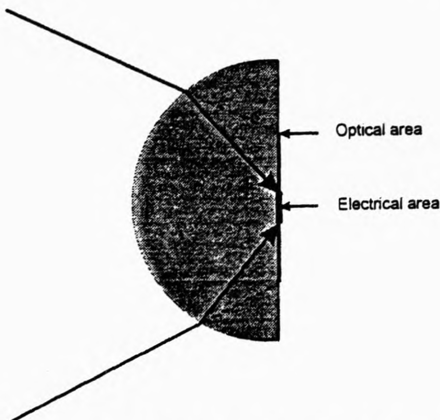

Fig. 7. Principle of optical immersion in the detector to a lens of high refractive index

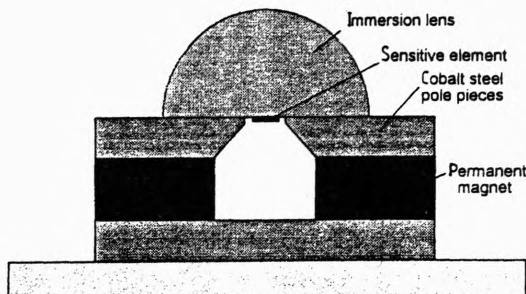

Fig. 8. Scheme of optically immersed magnetoconcentration detector

dissipation due to the immediate detector – substrate heat contact and pronounced 3-D heat transport.

An experimental optically immersed magnetoconcentration detector with monolithic immersion lens is shown in Fig. 8. The use of (Cd,Zn)Te hyperimmersion lens with refraction index results in improvement of detectivity by a factor of 7.

4. Recapitulation

The parameters of an uncooled $InAs_{1-x}Sb_x$ magnetoconcentration detector for the 10.6 μm CO_2 laser radiation have been calculated. It has been shown that the detectivity of such detector may achieve the value of $1 \cdot 10^9$ $cmHz^{1/2}/W$. The critical issue is the bias power dissipation. The necessary degree of depletion of semiconductor to suppress the Auger generation would require 10 W/mm^2 dissipation without any significant increase of detector temperature. Therefore, the use of optical immersion of a detector on an epitaxial layer to a lens formed in the substrate has been proposed to make the heat dissipation requirements less stringent and to achieve additional improvement of performance by a factor of 7.

References

[1] Catalogue VIGO Sensor SA, 1993.
[2] MALYUTENKO V. K., Phys. Status Solidi A **65** (1981), 131.
[3] DJURIČ Z., PIOTROWSKI J., Electron. Lett. **26** (1990), 1689.
[4] DJURIČ Z., PIOTROWSKI J., Proc. SPIE **1540** (1992), 1540.
[5] DJURIČ Z., PIOTROWSKI J., Opt. Eng. **31** (1992), 1955.
[6] DJURIČ Z., JAKSIČ Z., VUJANIČ A., PIOTROWSKI J., J. Appl. Phys. **71** (1992), 5706.
[7] PIOTROWSKI J., ROGALSKI A., *Półprzewodnikowe detektory podczerwieni* (in Polish), WNT, Warszawa 1985.
[8] ROGALSKI A., PIOTROWSKI J., Prog. Quantum Electron. **12** (1988), 87.
[9] ROGALSKI A., Prog. Quantum Electron. **13** (1989), 191.
[10] DOBBELAERE W., *Indium arsenide antimonide infrared detectors grown on gallium arsenide and silicon substrates by molecular beam epitaxy*, Interuniversitair Micro-Electronica Centrum vzw. Kapeldreef 75, B3001 Leuven, België, 1992.
[11] PIOTROWSKI J., Opto-Electronics Review **1** (1992), 9.
[12] GAWRON W., PIOTROWSKI J., *Ambient temperature IR photodetectors*, CLEO'92, Anheim, May 11 – 14, 1992.

Received December 3, 1992,
in revised form April 29, 1993